8-2022

Light Scattering Studies of Hyaluronate Solutions

Tim McNutt
txm7265@rit.edu

Light Scattering Studies of Hyaluronate Solutions

By

Tim McNutt

A thesis submitted in partial fulfillment of the requirements

for the degree of Master of Science in Physics, in the

College of Science, Rochester Institute of Technology.

August 2022

Approved by

Dr. George Thurston — Date

Director, M.S. Physics Program

Approval Committee:

PHYSICS

COLLEGE OF SCIENCE

ROCHESTER INSTITUTE OF TECHNOLOGY

ROCHESTER, NEW YORK

M.S. THESIS DEFENSE

Candidate: Tim McNutt

Thesis Title: Light Scattering Studies of Hyaluronate Solutions

Advisor: Dr. George Thurston

Date of defense: 8/10/2022

The candidate's M.S. Thesis has been reviewed by the undersigned. The Thesis

(a) is acceptable, as presented.

(b) is acceptable, subject to minor amendments.

(c) is not acceptable in its current form.

Written details of required amendments or improvements have been provided to the candidate.

Committee:

Dr. David Ross, Committee Member

Dr. Michael Kotlarchyk, Committee Member

Dr. Lishibanya Mohapatra, Committee Member

Dr. George Thurston, Thesis Advisor

Please submit form to Physics MS Graduate Program Coordinator

PHYSICS
COLLEGE OF SCIENCE
ROCHESTER INSTITUTE OF TECHNOLOGY
ROCHESTER, NEW YORK

CERTIFICATE OF APPROVAL

M.S. DEGREE THESIS

The M.S. Degree Thesis of *Tim McNutt* has been examined and approved by the thesis committee as satisfactory for the thesis requirement for the M.S. degree in Physics.

Dr. David Ross, Committee Member

Dr. Michael Kotlarchyk, Committee Member

Dr. Lishibanya Mohapatra, Committee Member

Dr. George Thurston, Thesis Advisor

Date

Acknowledgements

I want to acknowledge my family and friends for invaluable moral support and their continued love and acceptance of my work.

Abstract

The results of light scattering experiments on aqueous solutions of sodium hyaluronate are reported. Hyaluronate is an important component of the eye lens vitreous and many other connective tissues. The dependence of the light scattering on sodium hyaluronate molecular weight is studied and compared with a renormalization group model of polymer solution free energies. The results for the molecular weight and concentration ranges investigated fall on or near a universal scaling relationship provided by the model. This work extends previous comparisons of polyelectrolyte solutions to the same scaling relation.

Contents

1 Introduction

Hyaluronate is an important component within the body that can be found in the vitreous of the eye, synovial fluid of the knee and throughout the extracellular matrix (Karamanos *et al.*, 2018; Scott, 1992; Temple-Wong *et al.*, 2016). Along with its role as a key component of connective tissues, hyaluronate has multiple functions within the body including but not limited to wound healing, helping to trigger anti-inflammatory responses, and tissue homeostasis. It has been found that the effects of hyaluronate can change drastically depending on its molecular weight. An example is how hyaluronate in the range of 1000 kDa to 6000 kDa triggers anti-inflammatory properties, while in the range of 250 kDa to 1000 kDa it helps trigger pro-inflammatory responses (Tavianatou *et al.*, 2019).

Hyaluronate is a glycosaminoglycan (GAG) consisting of repeating disaccharide units of *N*-acetylglucosamine (GlcNAc) and glucuronic acid (GlcA). It is also a polyelectrolyte, because the carboxylate groups from glucuronic acid subunits make hyaluronate's overall charge negative. Polyelectrolytes contribute substantially to the swelling pressure of gels, through their effects on osmotic pressure (Hill, 1986). Thus characterizing the osmotic properties of hyaluronate as a function of molecular weight might contribute towards understanding observations that different hyaluronate molecular weights have different physiological effects.

Hyaluronate has been studied extensively due to its presence in almost all connective tissues in the body. As a result there is a lot of published literature about it, even when restricting the field of search to only light scattering. The second osmotic virial coefficients, A_2, have been determined for varying molecular weights with the solvent at a given ionic strength (Luan *et al.*, 2011). The effects of hyaluronate on osmotic pressure have also been explored at fixed molecular weights while varying the concentration of ions within the solvent; see for example Ghosh *et al.* (1990); Geissler *et al.* (2010).

The goal of characterizing how different molecular weights of hyaluronate affect osmotic pressure led to a comparison of the present data with a long-standing scaling model for the osmotic pressure of polymers, originated by Ohta & Oono (1982). Their model is well-supported by data relating osmotic pressure to concentration for varying polymer molecular weights

(Noda *et al.*, 1981; Wiltzius *et al.*, 1983).

In the Ohta and Oono model the osmotic pressure, Π, is rescaled so that the scaled osmotic pressure equals 1 for dilute solutions. That is, a rescaled value of 1 for osmotic pressure corresponds to the van 't Hoff law for the osmotic pressure of dilute solutions(Schroeder, 1999). The concentration is also scaled using the values of the second osmotic virial coefficient, A_2, and the molecular weight, M_w, of a given polymer. The Ohta-Oono rescaling creates a universal curve that was found to describe the dependence of osmotic pressure on concentration for a wide range of polymer molecular weights and second virial coefficients. The initial data for comparison came from solutions of poly(α-methylstyrenes) in toluene having a molecular weight range of 71 kDa to 7.5 MDa (Ohta & Oono, 1982; Noda *et al.*, 1981). Later, the corresponding osmotic compressibility scaling implied by the Ohta-Oono model was tested with use of light scattering of polystyrenes having 17.4 kDa $< M_w <$ 26 MDa, in both toluene and methyl ethyl ketone. Very good agreement was found (Wiltzius *et al.*, 1983), although it is also apparent that those data form their own scaling relation, which is quite close to the Ohta-Oono prediction. Subsequently, the model was also tested for its applicability to polyelectrolytes (Wang & Bloomfield, 1990). In particular, osmotic pressure data for aqueous solutions of sodium poly(styrenesulfonate), for 320 kDa $< M_w <$ 1.6 MDa were studied. These results also agreed well with the model developed by Ohta and Oono. The success of the Ohta-Oono scaling law for polyelectrolytes, found by Wang and Bloomfield, suggested that it could be valuable to compare the osmotic properties of hyaluronate with the same scaling law.

This work studies the effects of low molecular weights of hyaluronate, ranging from 5 kDa to 100 kDa, on osmotic compressibility, and compares the results with the Ohta-Oono scaling law. To do so, static light scattering is used to measure molecular weights, second osmotic viral coefficients, and more generally the osmotic compressibility. Although the molecular weights investigated here are generally smaller than the molecular weights typically reported for hyaluronate molecules in the body, such small molecular weights of hyaluronate are still present (Tavianatou *et al.*, 2019).

As mentioned, one of the quantities measured and reported here for hyaluronate is its

second virial coefficient, A_2. The second virial coefficient can help quantitate intermolecular interactions between pairs of molecules in imperfect gases and between solutes in a liquid. Equation (1.1) describes the second virial coefficient of a classical monatomic gas (Hill, 1986).

$$A_2 = -\frac{1}{4N_A}\int_0^\infty [e^{-u(r)/k_bT} - 1]4\pi r^2 dr \tag{1.1}$$

N_A is Avogadro's number and $u(r)$ is the potential between molecules. k_b is the Boltzmann constant, T is absolute temperature and r is the distance between the centers of two gas molecules, which are assumed in Eq.(1.1) to be spherically symmetric. Eq. (1.1) implies that ranges of r for which $u(r) < 0$ give negative contributions to A_2, and vice-versa for ranges for which $u(r) > 0$. Thus A_2 represents a balance between the influences of attractive and repulsive parts of $u(r)$.

Determining A_2 becomes more complex when considering multiple components in a solvent and a solute in a liquid solution. Equation (1.2) describes A_2 for a multicomponent solvent with a single solute. The main difference between Eq. (1.1) and Eq. (1.2) is the fact that one depends on $u(r)$ when the other depends on $w(r, z_\tau, T)$, the reversible work necessary to bring two solute molecules together from infinite separation. z_τ denotes a set of activity values (Hill, 1986), one for each solvent species.

$$A_2(z_\tau, T) = -\frac{1}{4N_A}\int_0^\infty [e^{-w(r,z_\tau,T)/k_bT} - 1]4\pi r^2 dr \tag{1.2}$$

Modeling A_2 from molecular properties becomes even more complex when charges and polymers are introduced, such as in the case of polyelectrolyte solutions. Factors including the extent of overlap between two neighboring polymers and charge screening then enter into the calculation of w (Hill, 1986). However the general relation between $u(r)$ or $w(r, z_\tau, T)$ and A_2 remains the same. As contrasted with modeling A_2 starting from the molecular structure of hyaluronate, analogous to the work of Bathe *et. al.* on chondroitin sulfate (Bathe, 2004), this thesis focuses on measurements of A_2. Such measurements can provide important points of reference for subsequent calculation and modeling.

The osmotic compressibility determined here represents one of several distinct contributions to the free energy of the complex gels found in connective tissues in the body (Hill, 1986). First, the contributions of other polyelectrolytes, notably collagen, must also be included and can be complex themselves; see for example Morozova & Muthukumar (2018). Second, the elasticity of the gel and the presence of free ions produce contributions (English *et al.*, 1996) that are not included in the present analysis. Third, components such as hyaluronate and collagen can also be present in chemically modified and cross-linked forms, and there are multiple other collagen and filament types present, for example in the eye vitreous (Sebag, 1998).

2 Methods

Making viable and usable samples for light scattering experiments turned out to be more challenging than expected when working with hyaluronate. The first hurdle to overcome was that there needed to be an accurate way to determine concentration of the samples. This was achieved by creating a calibration curve for hyaluronate with use of a UV-spectrophotometer.

The next challenge, as with all light scattering work, was to ensure that samples did not contain any dust. Dust was removed by following a systematic order of cleaning and filtration before taking light scattering measurements.

2.1 Calibration Curve

The calibration curve for hyaluronate was constructed by making multiple 1 ml samples of hyaluronate with a molecular weight of 5 kDa at various concentrations, ranging from 5 mg/ml down to 0.126 mg/ml, and taking UV absorbance measurements using a UV-spectrophotometer. The UV-spectrophotometer was set on its slowest setting and took a measurement every 0.1 nm. The UV-spectrophotometer was also baselined using the buffer the hyaluronate was in to ensure that only the hyaluronate absorbance was measured. The buffer was a 15 mM phosphate buffer with added NaCl, ionic strength 0.14 M, the same as for the light scattering samples. The resulting UV absorbance measurements can be seen in Figure 1.

The UV-spectrophotometer used starts to give a nonlinear response after the absorption exceeds a value of 1. Therefore the absorbance traces that stayed below 1 were used to create the calibration curve. Initially the small bump between wavelengths 256 nm and 287 nm in Figure 1 was chosen for use in calibration, because all such absorbances stayed below 1. However, the small bump was later found to be due to a contaminant in the samples. Subsequently, the larger peaks between 200 nm and 215 nm were used to make the calibration curve.

The next step was to transfer the data from the UV-spectrophotometer into Mathematica and to integrate the absorbance between 200 nm and 215 nm to determine how the area

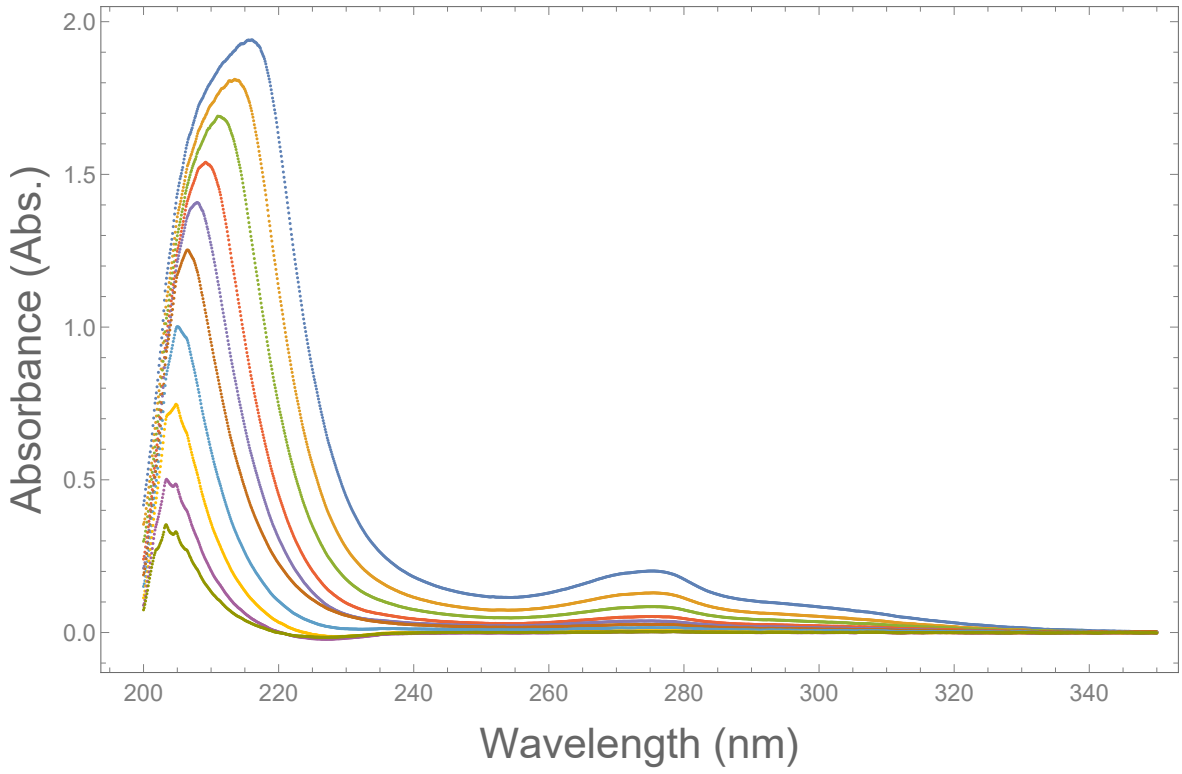

Figure 1: The UV-absorbance versus wavelength for varying concentrations of 5 kDa hyaluronate. The highest curve is for a concentration of 5 mg/ml, while the lowest is for a concentration of 0.126 mg/ml. Abs. stands for absorbance which is defined as $\log_{10}(I_\circ/I_T)$, where $I_\circ$ and I_T are the incident and transmitted intensities respectively.

changed as a function of concentration. Again, only absorbances below 1 were used, resulting in a calibration concentration range from 0.126 mg/ml to 0.429 mg/ml. The resulting relationship is shown in Figure 2b. Because the UV-spectrophotometer would give a nonlinear response after a sample concentration exceeded 0.5 mg/ml, samples were diluted by known degrees if needed for calibration. To use the calibration curve the integrated absorbance between between 200 nm and 215 nm was computed and then divided by the slope of the fitted line in Figure 2b, 21.9 $\pm$ 0.3 Abs.*nm/(mg/ml), to determine a sample's concentration of hyaluronate.

2.2 Sample Preparation

To make a viable light scattering sample the tube that the sample was going into was cleaned to be free of dust as much as possible. Because light scattering tubes were being

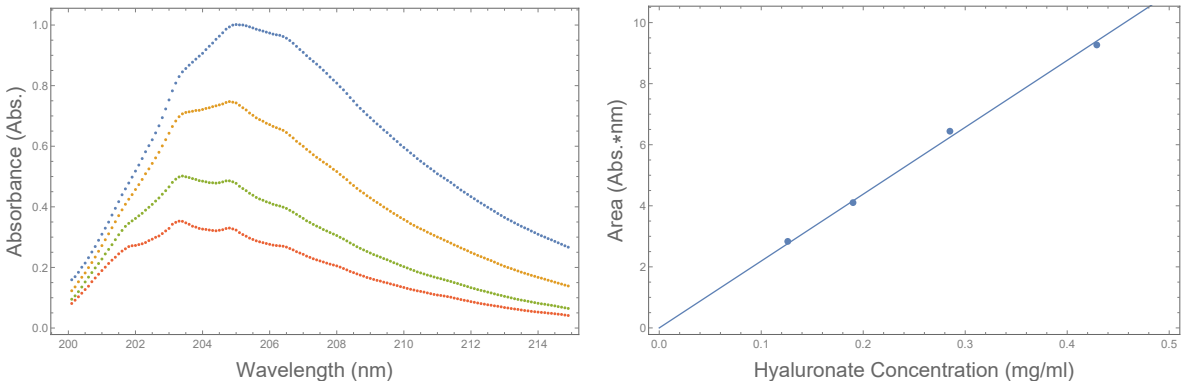

(a) (b)

Figure 2: (a) absorbance curves corresponding to the large peak in Figure 1 that stay below an absorbance value of 1. The concentrations of hyaluronate selected range from 0.429 mg/ml down to 0.126 mg/ml. (b) is the area underneath those curves versus concentration. A line is then fitted to the data using a least square fit with a slope of 21.9 ± 0.3 Abs.*nm/(mg/ml).

reused this was accomplished by washing the tubes in multiple baths for extended periods of time. The first bath used was a commercial detergent bath for 30 min, which was done to remove labels from the tubes easily and ensure that the acid and base baths did not need to be replaced as often. Then the tubes were placed in the base and acid baths for 24 hours each in that order. A 4 molar potassium hydroxide solution, which was then diluted to a 2 molar solution by adding ethanol until a 50/50 mix of water and ethanol was achieved was used for the base bath. A 4 molar nitric acid was used for the acid bath (Donovan *et al.*, 1991). Afterwards the tubes were rinsed with deionized water and left in a fume hood to dry before being used for light scattering again.

To make a light scattering sample, a washed light scattering tube was rinsed to ensure that any dust left over from the baths or that accumulated after being washed was removed. This was done by filling and emptying the tube with water having 18.2 MΩ∗cm resistivity up to 5 times. Then 1 ml of the same water was filtered through a 0.02 μm filter into the tube and the tube was put on a Fisher Vortex Genie 2 G560 set on vortex-3 for 30 seconds. The tube was covered with parafilm while on the Vortex Genie to make sure a spill did not occur in the lab. The tube was then rinsed one more time with 1 ml of filtered purified water. The tube was now ready for a hyaluronate sample to be added.

To make the hyaluronate solution for light scattering, the desired amount of hyaluronate was measured and placed in a 20 ml vial. The vial was not rinsed prior to this because the stock solution being made was later to be filtered into the light scattering tube. Then a 15 mM phosphate buffer with added NaCl, ionic strength 0.14 M, was filtered through a 0.02 μm filter into the vial until the desired amount by weight of buffer was added. The buffer recipe is detailed in Table B.1. The vial containing the hyaluronate was on a scale while adding the filtered buffer. For concentration calculations, it was assumed that the buffer had the same density as water. The buffer used as the solvent had the chosen ionic strength to better mimic ionic strength within tissue (Koushanpour, 1976). The hyaluronate solution was then placed on the Vortex Genie for 30 seconds on 'vortex-3' to speed the process of dissolving. For higher molecular weights and/or concentrations hyaluronate did not quickly dissolve by this method. In such cases samples were left overnight in the fridge to further dissolve before being transferred to a light scattering tube. For the molecular weights studied here, overnight was always enough time for the hyaluronate to dissolve so as to be ready for filtration into a light scattering tube.

While making light scattering samples, it was important to ensure that the masses of all components involved were well accounted for. This made it possible to see whether any of the solution evaporated overnight, or to still keep track of the concentration accurately if any complications occurred during the experiment, such as the need to replace a light scattering tube or a tube label.

After measuring the mass of the tube and the label being used the hyaluronate stock solution of a known concentration and given molecular weight was filtered into the tube through a 0.02 μm filter. The filters were from Whatman® Anotop®, Sigma-Aldrich product number WHA68091002. Then the sample was placed in the beam path of a 637 nm diode laser at 100 mW and visually checked for any significant dust remaining. A preliminary light scattering measurement of the sample was then taken to see if there was any dust that couldn't be seen by eye. This was apparent by looking at the count rate history of the measurement and seeing if there were any spikes in the data. If the spikes were thin, didn't happen too often and

the measurements returned to what was expected for a clean sample quickly the sample was considered viable. This was because the thin non-regular spikes could be removed from the data set by using the dust-cut off option built into the program being used, Brookhaven Instruments-Dynamic Light Scattering Software. Another check that was taken into account was that the range of the data collected, when stable, had to fall near what was expected following Poisson statistics. The light scattering sample of hyaluronate would then be left in the fridge overnight because having this rest period seemed to decrease the effect the remaining dust had on measurements. A light scattering sample that contained only the 15 mM phosphate buffer using the same process was also made, as well as a toluene sample. The toluene, spectrophotometric grade toluene (Sigma-Aldrich), was not filtered because it would dissolve the filters that were normally used. These additional samples were needed to assess the excess Rayleigh ratio of the hyaluronate samples, over that of the buffer.

There was one problem that occurred when trying to make samples at higher concentrations. When attempting to make samples above 7 mg/ml at 20 kDa, as well as for even lower concentrations at higher molecular weights, the 0.02 μm filters would break when preparing samples. To avoid this problem, the sample was filtered as before at lower concentrations, and then put into a centrifugal filtration device (Amicon® Ultra - 4, Ultracel® - 10k, Merck Millipore Ltd.). Filtration was performed at 5,000 g, where g is the force of gravity per unit mass, for 20 min at a time until the desired concentration was reached. Then the sample was pipetted into the light scattering tube.

2.3 Experimental Setup

All of the light scattering experiments conducted were performed with the same settings and same method. Brookhaven Instruments-Dynamic Light Scattering Software was used to control the power of a 637 nm diode laser and to collect and save data. The laser was a mini-L140 and a BI-200SM research goniometer was used to house the sample and hold the detector.

The detector angle was set at 90° for the static light scattering measurements because a

large angular dependence was not expected for these measurements. To check this assumption the following calculations were performed. First, a good approximation to the angular dependence of the scattered light for particles in the expected size range is that the fractional decrease of intensity with increasing angle is given by $\Delta R(\theta)/\Delta R(0) = (1+(1/3)(q(\theta)R_g)^2)^{-1}$, in which $\Delta R(\theta)$ is the excess Rayleigh ratio at scattering angle θ, and $\Delta R(0)$ is its value when extrapolated to scattering angle 0°. The excess Rayleigh ratio is to quantify the efficiency of light scattering and is used later in Section 3. $q = (4\pi n/\lambda_\circ)\sin(\theta/2)$ is the scattering vector magnitude and R_g is the radius of gyration. n is the index of refraction of the measured sample and $\lambda_\circ$ is the vacuum wavelength of incident light. n was kept constant for these estimates and was set to have the value for water, 1.33, which is what the pure buffer used is assumed to have. Figure 3 shows the estimated percent change for the planned molecular weights of hyaluronate to be used. R_g was estimated using $R_g = (C_l\xi_p/3)^{0.5}$, where C_l and ξ_p are the contour length and persistence length (Yamakawa, 1971). The contour length was estimated using the modeled length of an individual disaccharide unit from Bathe (2004) as 10.2 Å in combination with the known molecular weight of a disaccharide, 379 Da and the manufacturer's reported molecular weight. The persistence length used was 90 Å which was determined for hyaluronate in a solution of 0.1 M NaCl (Buhler & Boue, 2004), not far in ionic strength from the buffer used, 0.14 M.

The estimated values for each manufacturer's given molecular weight of hyaluronate are shown in Table 1. The results of estimating the angular dependence of the hyaluronate samples can be seen in Figure 3. $\Delta R(\theta)/\Delta R(0)$ for molecular weights below 38 kDa stays below an 3% change at 90°, while $\Delta R(\theta)/\Delta R(0)$ for 4.5 kDa doesn't exceed 0.5% over the range investigated. On the other hand $\Delta R(\theta)/\Delta R(0)$ for 119 kDa is around a 10% change at 90° and a 16% change at 140°. These results indicated that the angular dependence did not have a large effect for the lower molecular weights I was working with, but that the angular dependence would in principle need to be taken into account for the 119 kDa sample. Unfortunately the present 119 kDa samples were quite dusty for light scattering purposes, and accounting for angular dependence was not viable. Angular dependence was also not taken into account for the other

Part #	Lot	Manufacturer's M_w (Da)	Estimated C_l (Å)	Estimated R_g (Å)
HA 5K-1	028610	$4.6*10^3$	124	61
HA 20K-1	028292	$2.4*10^4$	646	139
HA 20K-1	028662	$3.8*10^4$	1023	175
HA 100K-1	028197	$1.19*10^5$	3202	310

Table 1: Information used to estimate C_l and R_g. A persistence length of 90 Å and a M_w of 379 Da per disaccharide unit was used.

hyaluronate samples.

The sample housing for experiments was regulated to be at (25 ± 0.02)°C by using a water cooling system and a Neslab water bath. The intensity of the laser was set at 100 mW and the aperture size was set at 400 μm. A one-hour delay was used between turning on the laser and water bath and taking measurements. This was done to ensure that the laser was stable and the sample housing was at thermal equilibrium. The chosen laser power and aperture provided for a substantial and practical difference in detected scattered light between dilute hyaluronate samples and the buffer.

Each session of measurements was started by taking a dark count measurement for 30 seconds, by closing the aperture with the laser on. Then measurements of scattering from toluene, then buffer were taken. These three measurements were done in this order because opening and closing the aperture multiple times was not desirable in order for the aperture to be in exactly the same position for the buffer, toluene, and hyaluronate samples. The toluene measurement was taken before the buffer measurement because the initial toluene measurement for the given day would give an idea of how much the buffer measurement should differ from past measurements of it on different days. The toluene measurement was repeated every hour in order to provide a secure reference for the other measurements. This was done by taking the ratio between the most recent toluene measurement and the initial one and then multiplying the initial buffer measurement by this ratio.

Following the initial reference measurements, hyaluronate samples were measured from 5 to 30 times depending on dust levels in the sample. The time for each measurement ranged from 30 seconds to 3 minutes. Once suitably clean measurements had been obtained, hyaluronate samples were diluted by adding buffer through a 0.02 μm filter. All dilution ratios were

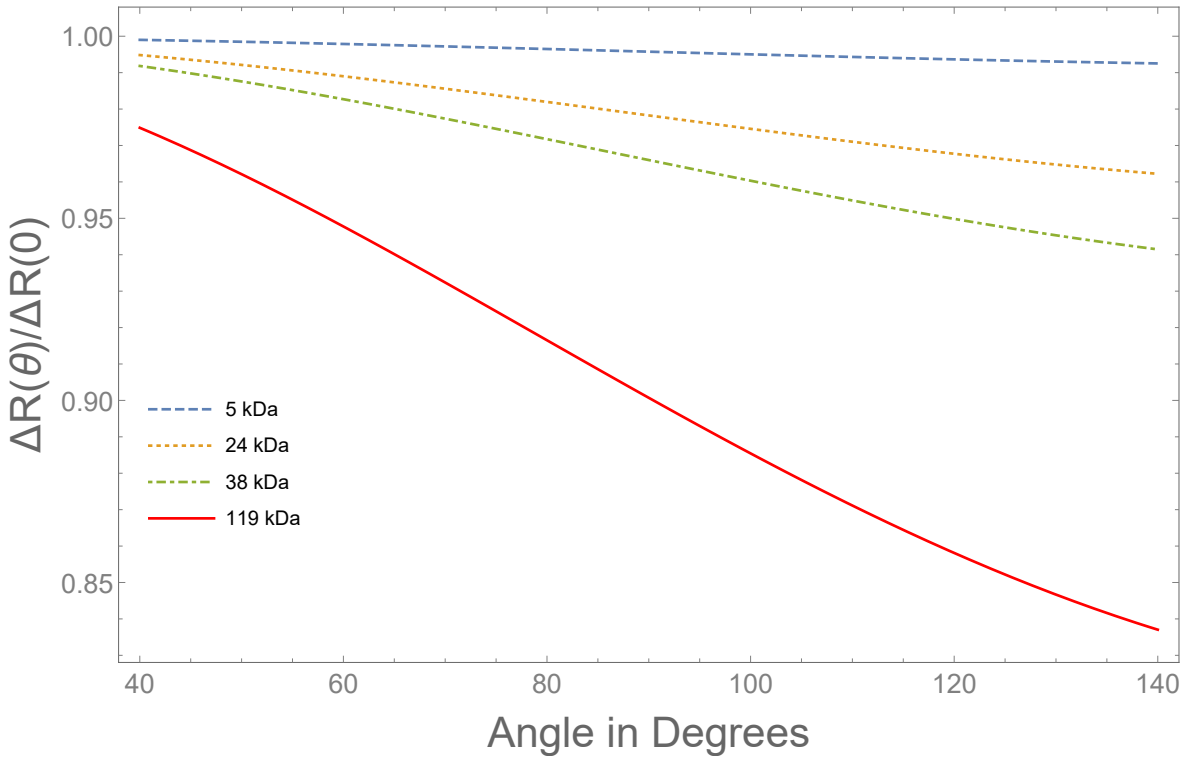

Figure 3: Predicted angular dependence of light scattering intensity as a function of hyaluronate M_w, as shown in the legend. The vertical line indicates the scattering angle used for the present measurements. See text.

determined by weighing, not volumetrically.

To guarantee that the sample was well mixed and properly diluted after adding the filtered buffer the sample was shaken and stirred gently by hand for a minute. Following this, further mixing was done with use of a Vortex Genie. To achieve gentle enough stirring, this was done at the setting of vortex-3 for one minute. If, instead, the sample had been vortexed too quickly, dust could have been introduced from the parafilm that was sealing the tube. Afterwards the sample was shaken and stirred gently again by hand for an additional minute. Usually this procedure was sufficient to fully mix the sample. However, once a repeatedly diluted sample started to reach the maximum volume possible in the tube, it may nevertheless have not yet been fully mixed. In order to check for this possibility, an initial light scattering measurement subsequent to the mixing was taken, to assess whether a reduction in intensity of the expected range had occurred. If not, the vortex intensity was increased and decreased periodically to further stir the sample. In more detail, the Vortex Genie setting was increased until a vortex started to form in the sample and was then decreased to the normal setting used, vortex-3. This process continued for another minute, and was followed by hand stirring. This procedure was usually sufficient for further measurements to proceed.

The repeated dilutions gave opportunities for dust to enter the sample. Therefore the dilution series was ended once the sample accumulated too much dust and was no longer viable, or at low enough concentrations so that the sample scattering was impracticably close to that of the buffer.

Figure 4 shows example count rates from experiments to illustrate the need for different measurement durations. Figure 4a shows a count-rate history from the hyaluronate sample having manufacturer's molecular weight 38 kDa. The measurement duration exceeded 2 minutes and the range of counts per second was close to 1 kcps. This range can be compared with what would be expected for a perfectly clean sample, for which Poisson counting statistics would apply. For the observed average count rate of 30.5 kcps, , a standard deviation of $\sigma = \sqrt{30500} = 1.75 \times 10^2$ would be expected. Therefore a range of $\pm 2\sigma$ on either side of the mean would include 700 cps, so that the observed range of close to 1 kcps is not too

much larger than what would be expected for Poisson statistics. In this example, the lack of numerous bumps or spikes enabled longer and therefore more accurate measurement of ΔR.

Figure 4b on the other hand shows a count-rate history taken from the hyaluronate sample with manufacturer's given molecular weight of 119 kDa. The range of count rates is clearly much larger than that shown in Figure 4a. Also, because of the many dust spikes, this measurement had to be shorter, 37 seconds, and the built-in software (Brookhaven Instruments-Dynamic Light Scattering Software) was used to remove the spikes in the data so that it could still be used for analysis. The software accomplished this by removing a batch of data if its intensity was higher than the average of the previous five batches plus the standard deviation of the five times the dust cutoff number, set to 20. Similar steps were taken for any sample that began to gather dust and become less viable over time. The shorter the duration of each measurement, more measurements were taken in total at a given concentration to obtain reliable estimates of the average count rate.

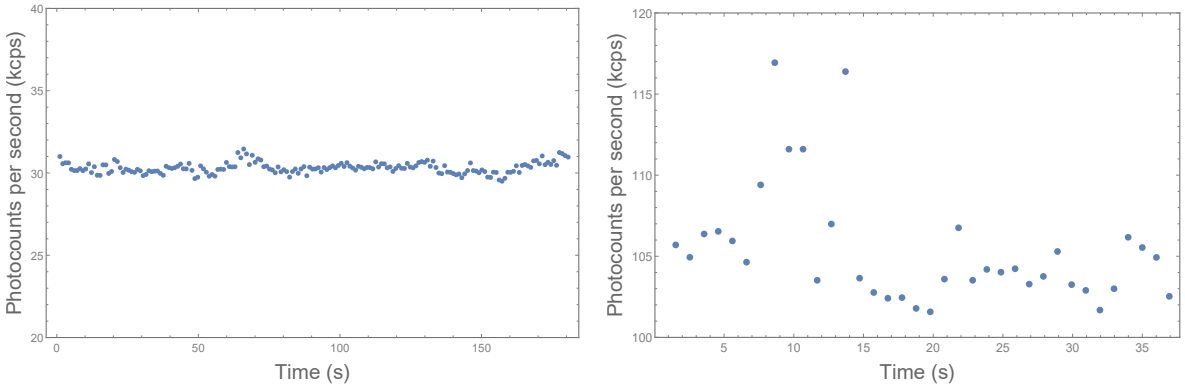

(a) (b)

Figure 4: (a) scattered light time dependence from a relatively clean sample, taken from a hyaluronate sample with given molecular weight 38 kDa. (b) is the same but from a relatively unclean but still usable sample, taken from a hyaluronate sample with given molecular weight 119 kDa. See text for more information.

3 Results

In this chapter the reference values used as well as the equations used to get the weight average molecular weight, M_w, and the second osmotic virial coefficient, A_2, for each light scattering sample are discussed. M_w was able to be determined for all measured hyaluronate (HA) samples. A_2 was able to be determined for all but one of the measured HA samples. This was due to not going up to high enough concentration for that sample.

The major difficulty faced when collecting the necessary data for determining the values of M_w and A_2 was that it took a significant period of time for a sample to be ready for light scattering, as mentioned in Chapter 2.

3.1 Obtaining A_2 and M_w

The two values that were plotted initially with the data were the excess Rayleigh ratios, ΔR, versus the corresponding concentration, c, of the HA samples. The Rayleigh ratios of HA solutions at differing concentrations were determined through comparison with scattered light from toluene using Eq. (3.3) (Coumou, 1960). Here, $\Delta I(90)$ is the excess of the photocount rate of light scattered from the solution to that of the buffer, and $I_{ref}(90)$ is the photocount rate of light scattered from toluene in excess of the dark count rate. n is the index of refraction of the HA solutions, which have the value of the index of water plus the change in index of refraction due to concentration of hyaluronate, $1.33 + c\frac{dn}{dc}$. n_{ref} is the index of refraction of toluene, 1.50 (Kaye & McDaniel, 1974). $\frac{dn}{dc}$ is the derivative of the hyaluronate solution index of refraction with respect to concentration. This value has been previously measured in the lab to be 0.137 ± 0.005 cm^3/g, by David Walls. That value is consistent with values reported in the literature for various HA solutions, which range from 0.136 cm^3/g to 0.157 cm^3/g.(Sorci & Reed, 2002; Walls, 2019). R_{ref} is the Rayleigh ratio of toluene, which has been accurately been determined in the past as $14.0*10^{-6}$cm^{-1} for a wavelength of 633 nm (Kaye & McDaniel, 1974). This was corrected using a $1/\lambda^4$ dependence of R_{ref} for use at the present wavelength, 637 nm, giving a R_{ref} value of $13.65*10^{-6}$cm^{-1}. In Eq.(3.3) $\Delta R(90)$ is the excess Rayleigh ratio at a scattering angle of 90°.

$$\Delta R(90) = \frac{\Delta I(90)}{I_{ref}(90)} R_{ref} \left(\frac{n}{n_{ref}} \right)^2 \tag{3.3}$$

Plots of excess Rayleigh ratio versus concentration were used while taking measurements to help determine if there were any obvious outliers possibly indicating that a given sample should be remeasured. An example of such a plot is shown in Figure 5a. Even though there were no obvious outliers in the data shown in Figure 5a, measurements were still taken at least 5 times at each concentration of hyaluronate to produce more reliable data. Multiple measurements were taken at a given concentration for all HA samples except in the case of the low molecular weight sample, lot 028610; see Table 2.

To determine the weight average molecular weight, M_w, and the second osmotic virial coefficient, A_2, $Kc/\Delta R$ versus concentration plots were created for each molecular weight and Eq. (3.4) was used. For this purpose, a commonly used form of the optical constant, K, was adopted, given by $K = 4\pi^2 n^2 (\frac{dn}{dc})^2 / N_A \lambda_\circ^4$. N_A is Avogadro's number and $\lambda_\circ$ is the vacuum wavelength of the incident light from our laser, 637 nm. M_w was determined using Eq. (3.4) by taking the inverse of the y intercept of the fitted function. A_2 was determined by dividing the slope of the fitted function by 2.

It is important to note that for the case of charged colloids, which includes polyelectrolytes such as the HA, Vrij & Overbeek (1962) published a thermodynamic analysis which included the influence of counterions on K. Briefly, they showed that the relevant refractive index increment, $(\frac{dn}{dc})$, should be evaluated at constant chemical potentials of all solutes except the colloid (Vrij & Overbeek, 1962). This correction was not attempted in the present work, for which the value of $(\frac{dn}{dc})$ used had been measured instead at constant concentrations of the other solutes.

When using Eq. (3.4) to determine M_w and A_2 the fitting parameters were limited to only the first two terms unless the Akaike information criterion (AIC) of the fit verified a noticeably better fit from including the next term (Cavanaugh & Neath, 2019), which would then yield the third osmotic virial coefficient, A_3. The fitting parameters were only extended to the third term of Eq. (3.4) for the HA sample with the given M_w of $2.4{*}10^4$ Da, lot 028292.

$$\frac{Kc}{\Delta R} = \frac{1}{M_w} + 2A_2c + 3A_3c^2 + \dots \tag{3.4}$$

Part #	Lot	Given M_w (Da)	Determined M_w (Da)	A_2 (mol*ml/g^2)
HA 5K-1	028610	4.6*10^3	(2.77±0.05)*10^3	n/a
HA 20K-1	028292	2.4*10^4	(3.09±0.13)*10^4	(3.89±0.03)*10^{-3}
HA 20K-1	028662	3.8*10^4	(3.99±0.08)*10^4	(5.59±0.04)*10^{-3}
HA 100K-1	028197	1.19*10^5	(1.33±0.02)*10^5	(2.57±0.07)*10^{-3}

Table 2: The hyaluronate used was from Lifecore Biomedical and their given lot numbers and molecular weights are shown in the table alongside the determined values from light scattering.

The graph of $Kc/\Delta R$ versus c for hyaluronate from lot 028662 is shown in Figure 5b. A table of determined M_w and A_2 values for differing HA samples is shown in Table 2. The error bars shown in plots here and below include the uncertainty of starting measurements, such as the initial masses of hyaluronate and solvent used, as well as propagated errors from including determined values in later analyses. An A_2 value for the sample with the given molecular weight of 4.6*10^3 Da, lot 028610, could not be determined from the data collected because the data did not extend to high enough concentrations.

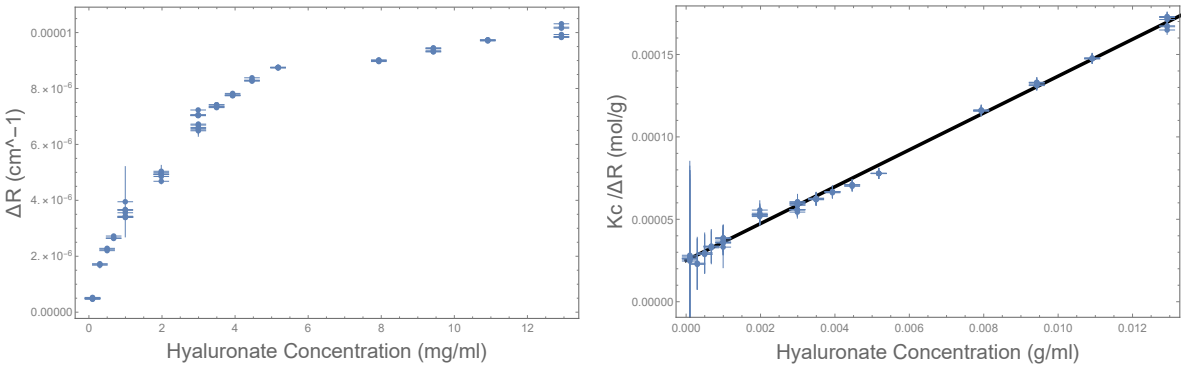

(a) (b)

Figure 5: (a) ΔR versus hyaluronate concentration for a manufacturer given M_w of 3.8*10^4 Daltons from lot 028662. (b) $Kc/\Delta R$ versus hyaluronate concentration for the same data. A linear fit yielded $M_w = (3.99 \pm 0.08)$*10^4 g/mol and $A_2 = (5.59 \pm 0.04)$*10^{-3} mol*ml/g^2.

Figure 6 shows the $Kc/\Delta R$ versus concentration plots for the samples from lots 028292 and 028197. A quadratic fit was used for the data of lot 028292 because the AIC indicated that it had a higher likelihood than the linear fit. For this sample, we find that $A_3 = 0.10 \pm$

0.02 mol*ml^2/g^3. The error in concentration in Figure 6b is more apparent than in Figure 6a and Figure 5 because the data were collected over a smaller concentration range. This resulted in a larger fractional concentration error than for the other data sets.

Figure 7 displays both the ΔR versus concentration as well as $Kc/\Delta R$ versus concentration plots for the sample from lot 028610 with manufacturer given M_w 4.6*10^3 Da, so as to better show why determining A_2 was not possible for this sample. To determine M_w, the slope of ΔR versus concentration was divided by K.

An interesting feature that stood out when looking at the data is that the error in ΔR and $Kc/\Delta R$ increases as concentration decreases. This is most likely due to the fact that the samples being measured became more dusty and therefore the standard deviation in the raw data collected increased greatly as concentration decreases, increasing the propagated error.

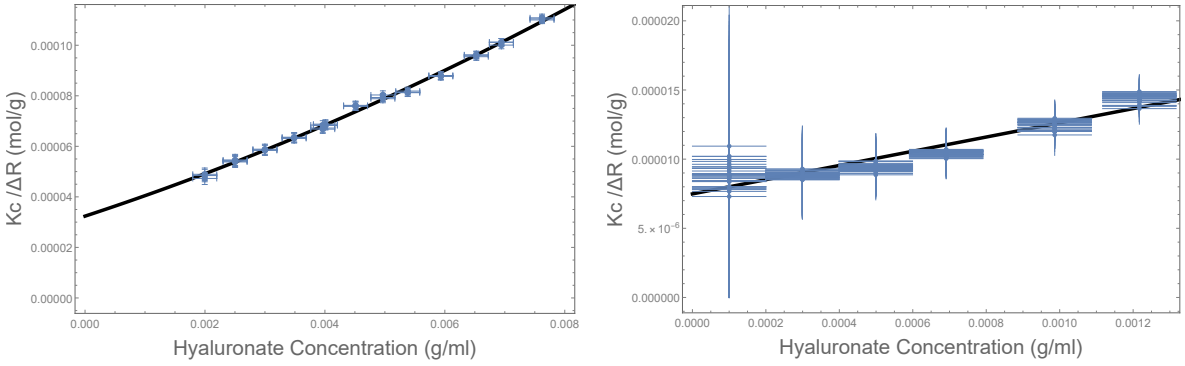

(a) (b)

Figure 6: (a) $Kc/\Delta R$ versus concentration of hyaluronate from lot 028292. A quadratic fit yielded a M_w of (3.09 $\pm$ 0.13)*10^4 g/mol and an A_2 of (3.89 $\pm$ 0.03)*10^{-3} mol*ml/g^2. (b) $Kc/\Delta R$ versus concentration of hyaluronate for lot 028197. A linear fit yielded a M_w of (1.33 $\pm$ 0.02)*10^5 g/mol and an A_2 of (25.7 $\pm$ 0.7)*10$^-$4 mol*ml/g^2.

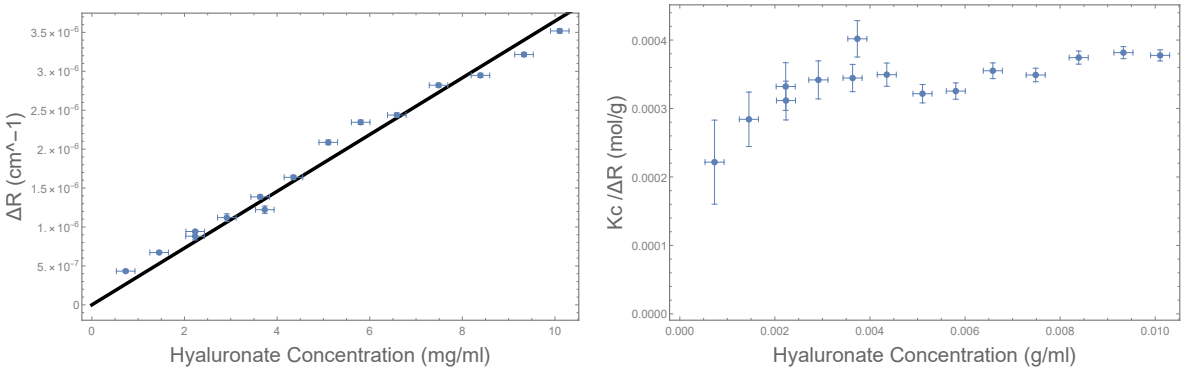

(a) (b)

Figure 7: (a) ΔR versus concentration of hyaluronate in for the sample with given manufacturer molecular weight 4.6*10^3 g/mol. M_w was determined to be (2.77 $\pm$ 0.05)*10^3 g/mol, see text for more information. (b) $Kc/\Delta R$ versus concentration of the same data as (a). An A_2 value could not be determined because the curve for the $Kc/\Delta R$ graph did not have a clear slope and adding more terms to the fit would not make it reliable.

4 Analysis

4.1 Overview

A_2 values were compared to data collected by Luan *et al.* (2011), whose results were chosen for comparison because the molecular weight range overlapped with that being investigated in this study.

The present light scattering data were also compared with a proposed universal model for the scaling of osmotic pressure with concentration for polymers. Although the model was initially designed for polymers, it was also shown that it can be applied to polyelectrolytes (Ohta & Oono, 1982; Wang & Bloomfield, 1990; Wiltzius *et al.*, 1983). Knowing this, we wanted to see whether hyaluronate follows this model as well.

The main difficulty in doing so was taking the already existing data and putting it in a scaled form that would match the model. To make it so the data could be compared to the mentioned model the data needed to be scaled using the already determined values, M_w and A_2. How this was done will be laid out later in the chapter.

4.2 Comparing A_2 Values to Literature

Luan *et al.* (2011) reported $\log(A_2)$ versus $\log(M_w)$ for hyaluronate in the molecular weight range 10^4 Da to 10^6 Da. Their work showed that the log-log trend of A_2 versus M_w is linear with a slope of -0.19 $\pm$ 0.02, which agreed well with predictions and past experiments (Cowman & Matsuoka, 2005; Takahashi *et al.*, 2003).

Figure 8 shows a comparison of the present data with those reported by Luan *et al.* (2011). The circles are Luan's data while the data collected in this study are the squares, with error bars. Figure 8 shows that the present data is quite consistent with Luan's results. Note that Luan *et al.* (2011) used 0.1M NaCl, slightly different from our buffer ionic strength of 0.14M. Also, angular dependence was not taken into account in the present study, unlike that of Luan *et al.* (2011).

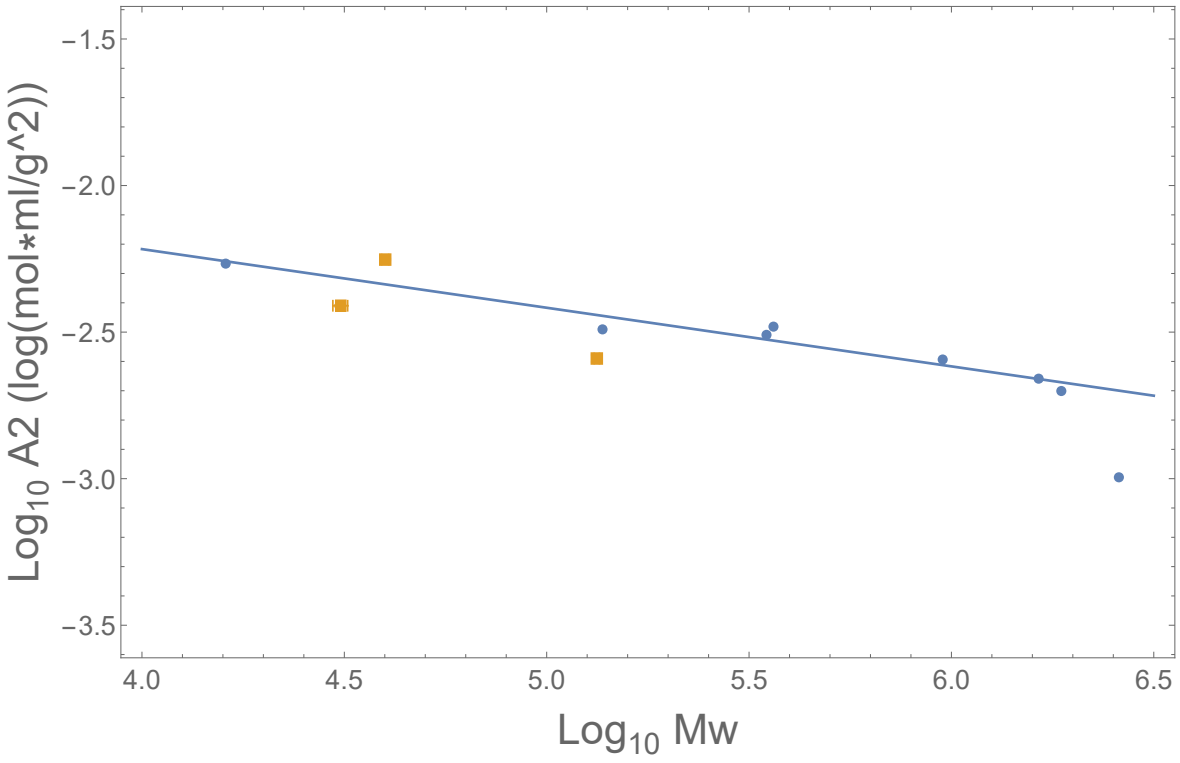

Figure 8: $\mathrm{Log}_{10}A_2$ versus $\mathrm{Log}_{10}M_w$. The blue circles and the line, having slope -0.19 ± 0.02, are from Luan *et al.* (2011) and the yellow squares are the present data.

4.3 The Model

In 1982 Ohta and Oono developed a universal curve for the osmotic pressure versus number density of polymers, described in Eq. (4.7) (Ohta & Oono, 1982). On the left hand side Π is the osmotic pressure, ρ is the number density of solute, k_b is the Boltzmann constant, and T is the absolute temperature.

$$X\Big[\frac{9}{16} - \ln\left(\frac{M_w}{M_n}\right)/8\Big] = A_2 M_w c \tag{4.5}$$

$$\mu = \frac{M_n}{M_w} \tag{4.6}$$

$$\frac{\Pi}{\rho k_b T} = 1 + \frac{1}{2}X\exp\left(\frac{1}{4}\epsilon\Big[\frac{\mu}{X} + \frac{\mu^2}{X^2}\ln\mu + \left(1 - \frac{\mu^2}{X^2}\right)\ln(X+\mu)\Big]\right) \tag{4.7}$$

On the right hand side X is a dimensionless form of reduced concentration of solute shown in Eq. (4.5), ϵ is $4 - d$, where d is the number of spatial dimensions, so in our case ϵ is equal to 1. $\mu = M_n/M_w$ is the inverse of the commonly defined polydispersity index, PDI $= M_w/M_n$, in which M_n is the number average molecular weight and M_w is the weight average molecular weight. For convenience, X is represented here as a function of weight per unit volume concentration, c, whereas Ohta & Oono (1982) instead used number density, ρ.

The model developed by Ohta and Oono was originally compared to experimental data reported by Noda *et al.* (1981) for poly(α-methylstyrene) in toluene at 25°C. The data for this uncharged polymer agreed well with the model, for polymer molecular weight range of 71 kDa $< M_w <$ 7.5 MDa and for $0.05 < X <\sim 10$.

Following this initial comparison, Wiltzius *et al.* (1983) used static light scattering to extend the comparison to the corresponding scaling prediction for osmotic compressibility, $(\frac{\partial\Pi}{\partial c})$, shown in Eq.(4.8) (Wiltzius *et al.*, 1983). They also used an uncharged polymer, polystyrene, in the solvents toluene and methyl ethyl ketone. In Eq.(4.8) M_w and N_A appear as a result of changing from number density, ρ, to concentration, c. The data of Wiltzius *et al.* (1983) showed a scaling of their own, which was also close to that predicted by the Ohta and Oono

model, for 17.5 kDa $< M_w <$ 26 MDa and $0.05 < X < 50$.

$$\frac{M_w}{N_A k_b T}\left(\frac{\partial \Pi}{\partial c}\right)_T = 1 + \frac{1}{8}\left[9X - 2 + \frac{2\ln(1+X)}{X}\right]\exp\left(\frac{1}{4}\left[\frac{1}{X} + \left(1 - \frac{1}{X^2}\right)\ln(1+X)\right]\right) \tag{4.8}$$

Equation (4.8) includes the assumption that $\mu = 1$, meaning that the sample is monodisperse. Wiltzius chose the PDI to be 1 because X differed by less than 6% between the then relevant PDI values 1 and 1.3 (Wiltzius *et al.*, 1983). Because the PDI values relevant here were larger, ranging from 1.4 to 1.9, the effects of polydispersity on the model and the data from the present study were investigated and are described below in section 4.4.

Later the Ohta and Oono model was compared to several polyelectrolytes, including poly(styrenesulfonate) (Wang & Bloomfield, 1990). The osmotic pressure, as predicted by Equation (4.7), was shown to accurately model the change in the normalized osmotic pressure as a function of poly(styrenesulfonate). These results on poly(styrenesulfonate) suggested comparing the present polyelectrolyte, hyaluronate, to the model, by making use of the osmotic compressibility obtained from static light scattering.

4.4 Compare Results to the Model

To use Eq. (4.8) it was necessary to relate $(\frac{\partial \Pi}{\partial c})$ to ΔR. The first step was to relate ΔR to the free energy by Eq. (4.9)(Bell *et al.*, 2017). Note that in the free energy formulation used here, the solvent is being treated as if it were a single component. Thus, the free energy contributions of free ions and counterions are not included. Consequently, the osmotic pressure and compressibility reported here can be taken to represent that due to the hyaluronate alone, and further analysis is needed to include ionic contributions.

$$\Delta R(\theta) = \left(\frac{\pi^2 k_b T}{\lambda_\circ^4}\right)\nabla_\rho \epsilon^{T'} \cdot H_\rho[G/V]^{-1} \cdot \nabla_\rho \epsilon \tag{4.9}$$

$H_\rho[G/V]$ is the Hessian matrix of second partial derivatives of the Gibbs free energy per unit volume, V, with respect to the number densities of the components. $\nabla_\rho \epsilon$ is the gradient of the dimensionless dielectric coefficient, ϵ, with respect to number densities, ρ at the incident wavelength (Bell *et al.*, 2017). T' signifies the transpose of the gradient. Equation (4.9) though

is for more than one solute in solution and therefore can be simplified for our case with only hyaluronate in solution.

The first step was to simplify the Hessian matrix in Eq.(4.9) to apply to a single component, as in Eq. 4.10. This was taken a step further by putting G in a dimensionless form g, defined in Eq. 4.11 where Ω_w is the volume of a water molecule. ρ was put instead in terms of volume fraction, η, as in Eq. 4.12, in which N_s is the number of solute molecules, η_s is the volume fraction of solute in solution and Ω_s is the volume of a solute molecule. These substitutions resulted in Eq. (4.13).

$$H_\rho[G/V]^{-1} = \left(\frac{\partial^2(G/V)}{\partial\rho_1^2}\right)^{-1} \tag{4.10}$$

$$g = \frac{\Omega_w G}{k_b T V} \tag{4.11}$$

$$\rho = \frac{N_s}{V} = \frac{\eta_s}{\Omega_s} \tag{4.12}$$

$$\left(\frac{\partial^2(G/V)}{\partial\rho_1^2}\right)^{-1} = \frac{\Omega_w}{\Omega_s^2 k_b T}\left(\frac{\partial^2 g}{\partial\eta_s^2}\right)^{-1} \tag{4.13}$$

The next part of Eq. (4.9) that was simplified was $\nabla_\rho\epsilon$. This was done using Eq. (4.14) where the transpose of $\nabla_\rho\epsilon$ for two components is defined (Bell *et al.*, 2017). m_1 and m_2 are the masses of the two components molecules while c_1 and c_2 are their respective concentrations in solution. Equation (4.14) can be simplified for one component by removing all terms that refer to a second component.

$$\nabla_\rho\epsilon^{T'} = \left(\frac{\partial(n^2)}{\partial\rho_1}, \frac{\partial(n^2)}{\partial\rho_2}\right) = 2n\left(m_1\frac{\partial n}{\partial c_1}, m_2\frac{\partial n}{\partial c_2}\right) \tag{4.14}$$

Taking Eqs. (4.13) and (4.14) and substituting them into Eq. (4.9) leads to Eq. (4.15) where any additional indices were dropped because this is for one component in solution. From here only a few more substitutions needed to be done to relate the determined values to the

left hand side of Eq. (4.8).

$$\Delta R(\theta) = \frac{\pi^2}{\lambda_\circ^4} 4n^2 \left(\frac{\partial n}{\partial c}\right)^2 \frac{m_s^2 \Omega_w}{\Omega_s^2} \left(\frac{\partial^2 g}{\partial \eta_s^2}\right)^{-1} \tag{4.15}$$

$$\frac{\Pi \Omega_w}{k_b T} = \frac{\mu_w^\circ}{k_b T} - g + \eta_s \frac{\partial g}{\partial \eta_s} \tag{4.16}$$

In the appendix it is shown that upon taking the derivative of Eq. (4.16) with respect to η_s, substituting into Eq. (4.15), and rearranging leads to Eq. (4.17):

$$\left(\frac{\partial \Pi}{\partial \eta_s}\right)_T = \frac{\pi^2}{\Delta R \lambda_\circ^4} 4n^2 \left(\frac{\partial n}{\partial c}\right)^2 \frac{m_s^2}{\Omega_s^2} k_b T \eta_s \tag{4.17}$$

Substituting the definition of K into Eq. (4.17) and using the relation that $c(\Omega_s/m_s) = \eta_s$, $\partial\Pi/\partial\eta_s$ can be expressed in terms of ΔR, K, and c, and then substituted into the left hand side of Eq. (4.8). This results in Eqs. (4.18) and (4.19):

$$\left(\frac{\partial \Pi}{\partial c}\right)_T = \frac{Kc}{\Delta R} N_A k_b T \tag{4.18}$$

$$\frac{M_w}{N_A k_b T} \left(\frac{\partial \Pi}{\partial c}\right)_T = \frac{K c M_w}{\Delta R} \tag{4.19}$$

Eqs. (4.19) and Eq. (4.5) indicate that to compare the collected data with the model of Eq. (4.8), one needs to scale the $Kc/\Delta R$ data versus the scaled concentration X, which incorporates A_2 and M_w. Consequently the data for $M_w = 4.6 * 10^3$ Da could not be evaluated in this manner, because A_2 was not determined as described above.

Note that Eq. (4.7) indicates that the original Ohta-Oono scaling model depends on the polydispersity of the sample, while Wiltzius *et. al.* set the polydispersity to 1 in Eq. (4.8). As indicated above, they reported that this assumption made for a difference in X values of less than 6% for the maximum PDI of 1.3 relevant for their studies. In the present case, however, the manufacturer of the hyaluronate used here reported its PDI as ranging from 1.4 to 1.9. This warranted checking whether or not including polydispersity in the model would

make a significant change. Eq.(4.20) shows the polydispersity-dependent counterpart of the scaled osmotic compressibility equation presented above, Eq.(4.8); setting $\mu = 1$ in Eq.(4.20) reproduces Eq.(4.8)

$$\frac{M_w}{N_A k_b T}\left(\frac{\partial \Pi}{\partial c}\right)_T = X \exp\left(\frac{1}{4}\left(\frac{\mu^2 \ln(\mu)}{X^2} + \left(1 - \frac{\mu^2}{X^2}\right)\ln(\mu + X) + \frac{\mu}{X}\right)\right) + \frac{1}{8} X \left(-\frac{3\mu^2 \ln(\mu)}{X^2} + \frac{2\mu \ln(\mu + X)}{X^2} - \frac{2\mu}{X} + 1\right) \exp\left(\frac{1}{4}\left(\frac{\mu^2 \ln(\mu)}{X^2} + \left(1 - \frac{\mu^2}{X^2}\right)\ln(\mu + X) + \frac{\mu}{X}\right)\right) + 1 \tag{4.20}$$

With use of Eq.(4.20), the effect of polydispersity was checked by comparing the scaling plot for hyaluronate with determined M_w (1.33 ± 0.02)*10^5 Da, using both the manufacturer's reported PDI of 1.6 ($\mu = 0.625$) and a hypothetical PDI of 1.0 ($\mu = 1.0$). The resulting plot is shown in Figure 9. The combination of Eqs.(4.5) and (4.20) indicates that for values of $\mu \neq 1$ data points will be shifted both horizontally and vertically, respectively. The dashed line in Figure 9 shows how the model changes for a μ of 0.625, and shows that the changes in the model are relatively small for polydispersity of this magnitude. Figure 9 also shows that the scaled data for M_w (1.33 ± 0.02)*10^5 is close to the Ohta-Oono model with or without the inclusion of $\mu \neq 1$. It should be noted that both in Wiltzius' work and Wang and Bloomfield's work the relevant data also does not fall exactly on the Ohta-Oono scaling curve, but nevertheless follows its general trend (Wiltzius *et al.*, 1983; Wang & Bloomfield, 1990).

All data that were able to be suitably scaled are plotted in Figure 10; some data points at very low concentrations were removed because the errors in X became larger than X itself. These errors were primarily due to dust in multiply-diluted samples near the end of dilution series.

Figure 10 clearly shows that hyaluronate in the investigated molecular weight range, 31 kDa $< M_w <$ 133 kDa, for the ionic strength of 0.14 M used here, falls near the Ohta-Oono scaling curve. At the same time, it is also apparent that hyaluronate data at higher values of X are needed to evaluate the extent to which this remains the case. It is important to note

that in constructing both Figs. 9 and 10 there is no fitting aside from the experimental data reduction described above. That is, there are no adjustable parameters involved in creating either figure.

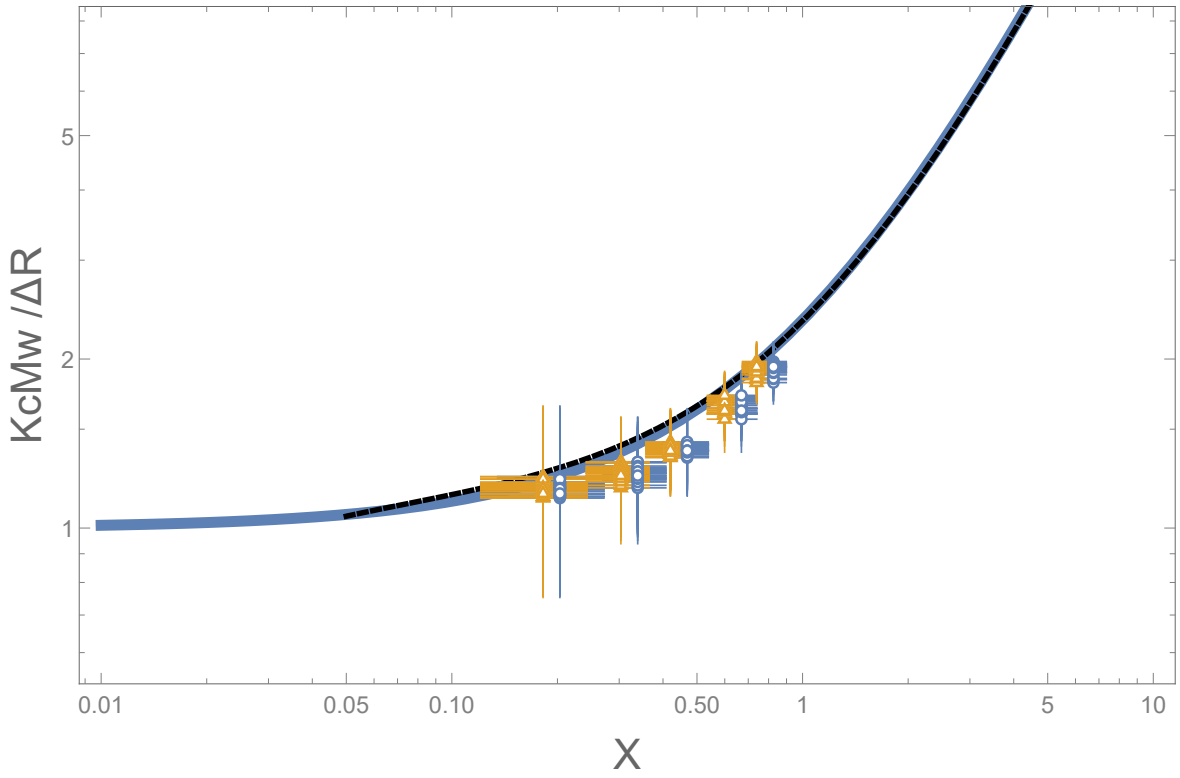

Figure 9: $KcM_w/\Delta R$ versus X on log scales of the data from hyaluronate with determined M_w, (1.33 ± 0.02)*10^5 g/mol. The circles are for PDI = 1.6 and the triangles are for PDI = 1.0. The dashed line shows the Ohta-Oono scaling relation calculated for PDI = 1.6. See text.

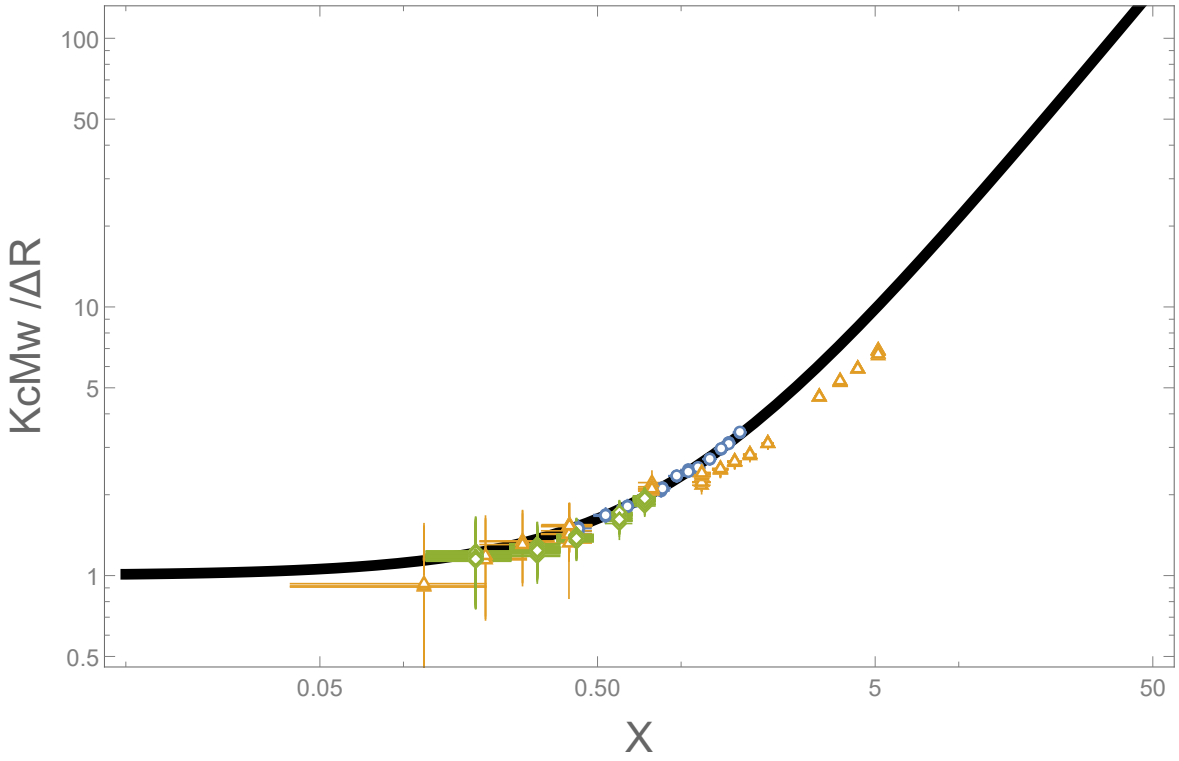

Figure 10: All data collected, except for that on lot 028610, are scaled and plotted here alongside the model from Eq. (4.8), assuming a polydispersity index of 1.0 (see text). The circle, triangle and diamond markers are for data sets with determined molecular weights (3.09 ± 0.13)*10^4 g/mol, (3.99 ± 0.08)*10^4 g/mol, and (1.33 ± 0.02)*10^5 g/mol respectively.

5 Conclusions

First, the values determined for the various molecular weights of hyaluronate investigated here were close to those given by the manufacturer, as shown in Table 2.

Second, the corresponding values for the second virial coefficient A_2 were found to be in agreement with previous data (Luan *et al.*, 2011).

Third, the present hyaluronate solutions showed static light scattering data which was close to a proposed scaling relation for the osmotic compressibility of polymer solutions. This relation is implied by one proposed for osmotic pressure (Ohta & Oono, 1982). Further work is needed to extend the comparison to higher values of scaled hyaluronate concentration, X, to higher molecular weights, M_w, as well as to investigate the corresponding quasielastic light scattering. Investigation of higher molecular weights will require probing the angular dependence of the scattering, as indicated by the calculations displayed in Figure 3.

As mentioned in the Introduction, the osmotic compressibility determined here reflects one contribution to the free energy of complex gels found in connective tissues in the body. The scaling relationship suggested by the present work, if further verified as indicated above, would permit quantitative modeling of the corresponding free energy contributions for a broad variety of hyaluronate molecular weights. At the same time, as also mentioned, it is important to note that contributions from other polyelectrolytes, cross-links, and ions also contribute to the free energy.

Appendices

Appendix A

Relating Osmotic Pressure to Free Energy

The steps taken to relate g, dimensionless form of the Gibbs Free energy, to Π, the osmotic pressure, are found below. First, it should be stated that P for pressure in gas equations of state is analogous to Π when dealing with a liquid solution. Because one commonly considers the liquid and its constituents as being incompressible the following equation can be used:

$$\Pi * \Omega_w = \mu_w^\circ - \mu_w \tag{A.1}$$

where Π is the osmotic pressure, Ω_w is the volume of a water molecule, μ_w° is the chemical potential of pure water and μ_w is the actual water chemical potential at a finite solute concentration. The pure buffer solution will be treated as having the same chemical potential as pure water.

$$dG = -SdT + VdP + \mu_w dN_w + \mu_s dN_s \tag{A.2}$$

Equation (A.2) is the fundamental relationship of the Gibbs's free energy. It should be noted that μ_s and N_s are the chemical potential of solute in solution and the number of solute molecules in solution respectively. Equation (A.2) can also give the following:

$$\left.\frac{\partial G}{\partial N_w}\right|_{T,P,N_s} = \mu_w \tag{A.3}$$

For this work a relation to a dimensionless version of the free energy was preferred, which can be written as follows:

$$g = \frac{\Omega_w G}{k_b T V} \tag{A.4}$$

V in Eq. (A.4) is defined in Eq. (A.5). It is also useful to define a variable for the volume fraction of the solute in solution, which is defined in Eq. (A.6). Equations (A.6) through (A.8) are simple steps that are needed to continue.

$$V = N_w\Omega_w + N_s\Omega_s \tag{A.5}$$

$$\eta_s = \frac{\Omega_s N_s}{V} \tag{A.6}$$

$$\eta_w = 1 - \eta_s \tag{A.7}$$

$$\frac{\partial g}{\partial \eta_s} = \frac{\partial g}{\partial \eta_w}\frac{\partial \eta_w}{\partial \eta_s} = -\frac{\partial g}{\partial \eta_w} \tag{A.8}$$

To move forward $\frac{\partial g}{\partial \eta_p}$ needs to be related to the partial derivative in Eq. (A.3). One way to accomplish this is by solving for $\frac{\partial g}{\partial N_w}$ at constant N_s.

$$\left.\frac{\partial g}{\partial N_w}\right|_{N_s,P,T} = \left.\frac{\partial g}{\partial \eta_w}\frac{\partial \eta_w}{\partial N_w}\right|_{N_s,P,T} \tag{A.9}$$

Using Eqs. (A.5) and (A.6), with using the water volume fraction, the Eq. (A.9) equals what is below:

$$= \frac{-\partial g}{\partial \eta_s}\left(\frac{\Omega_w}{\Omega_w N_w + \Omega_s N_s} - \frac{\Omega_w N_w \Omega_w}{(\Omega_w N_w + \Omega_s N_s)^2}\right) \tag{A.10}$$

Which than can be simplified further as:

$$= \frac{-\partial g}{\partial \eta_s}\left(\frac{\Omega_w}{V}\right)(1-(1-\eta_s)) \tag{A.11}$$

Which can further be simplified as:

$$\left.\frac{\partial g}{\partial N_w}\right|_{N_s,P,T} = -\eta_s\left(\frac{\Omega_w}{V}\right)\frac{\partial g}{\partial \eta_s} \tag{A.12}$$

$\frac{\partial g}{\partial N_w}$ could have been solbed by directly substituting in the definition for g.

$$\left.\frac{\partial g}{\partial N_w}\right|_{N_s,P,T} = \frac{\partial}{\partial N_w}\left(\frac{\Omega_w G}{k_b T V}\right)_{N_s,P,T} \tag{A.13}$$

$$= \frac{\Omega_w}{k_b T}\left(\frac{\partial}{\partial N_w}\left(\frac{G}{\Omega_w N_w + \Omega_s N_s}\right)\right)_{N_s,P,T} \tag{A.14}$$

$$= \frac{\Omega_w}{k_b T}\left(\frac{(\frac{\partial G}{\partial N_w})_{N_s,P,T}}{V} - \frac{G\Omega_w}{V^2}\right) \tag{A.15}$$

Using Eq. (A.3) the above can be simplified to:

$$= \frac{\Omega_w}{V k_b T}\left(\mu_w - \frac{G\Omega_w}{V}\right) \tag{A.16}$$

Setting Eqs. (A.12) and (A.16) equal to one another leads to the following.

$$\frac{\Omega_w}{V}\left(\frac{\mu_w}{k_b T} - g\right) = -\eta_s\left(\frac{\Omega_w}{V}\right)\frac{\partial g}{\partial \eta_s} \tag{A.17}$$

Which results to the following:

$$\frac{\mu_w}{k_b T} = g - \eta_s \frac{\partial g}{\partial \eta_s} \tag{A.18}$$

Then dividing Eq. (A.1) by K_bT and using Eq. (A.18) one can set up what follows, the relation for Π and g:

$$\frac{\Pi\Omega_w}{k_bT} = \frac{\mu_w^\circ}{k_bT} - g + \eta_s \frac{\partial g}{\partial \eta_s} \tag{A.19}$$

Appendix B

Chemical Recipes

Chemical	Molarity	Supplier
Na_2HPO_4	0.01017	Fisher Scientific
NaH_2PO_4	0.00512	Sigma-Aldrich
NaCl	0.10560	Sigma-Aldrich

Table B.1: The chemicals used to make the 15 mM phosphate buffer at around 0.14 M ionic strength are shown above. It should be noted that the NaCl used was ACS grade.

Chemical	Molarity	Supplier
KOH	2	VWR
HNO_3	4	VWR

Table B.2: Prior to placing tubes in the acid and base baths the tubes were soaked in a detergent bath for between 15-30 min. Liquinox from Alconox was used for the detergent. When making the base bath we first made a 4 M solution with pure water and then added 200 proof pure ethanol to make it 2 M. The ethanol was from Koptec. The HNO_3 was between 69% and 70% and was ACS grade.

Bibliography

Bathe, Mark. 2004. *Inverse Monte Carlo simulation of biomolecular conformation and coarse-grained molecular modeling of chondroitin sulfate conformation, titration, and osmotic pressure.* Ph.D. thesis, Massachusetts Institute of Technology. 1, 2.3

Bell, Michael M, Ross, David S, Bautista, Maurino P, Shahmohamad, Hossein, Langner, Andreas, Hamilton, John F, Lahnovych, Carrie N, & Thurston, George M. 2017. Statistical-thermodynamic model for light scattering from eye lens protein mixtures. *The Journal of Chemical Physics*, **146**(5), 055101. 4.4, 4.4, 4.4

Buhler, Eric, & Boue, Francois. 2004. Chain persistence length and structure in hyaluronan solutions: Ionic strength dependence for a model semirigid polyelectrolyte. *Macromolecules*, **37**(4), 1600–1610. 2.3

Cavanaugh, Joseph E, & Neath, Andrew A. 2019. The Akaike information criterion: Background, derivation, properties, application, interpretation, and refinements. *Wiley Interdisciplinary Reviews: Computational Statistics*, **11**(3), e1460. 3.1

Coumou, DJ. 1960. Apparatus for the measurement of light scattering in liquids: Measurement of the Rayleigh factor of benzene and of some other pure liquids. *Journal of Colloid Science*, **15**(5), 408–417. 3.1

Cowman, Mary K, & Matsuoka, Shiro. 2005. Experimental approaches to hyaluronan structure. *Carbohydrate research*, **340**(5), 791–809. 4.2

Donovan, JM, Timofeyeva, N, & Carey, MC. 1991. Influence of total lipid concentration, bile

salt: lecithin ratio, and cholesterol content on inter-mixed micellar/vesicular (non-lecithin-associated) bile salt concentrations in model bile. *Journal of lipid research*, **32**(9), 1501–1512. 2.2

English, Anthony E, Mafé, Salvador, Manzanares, José A, Yu, Xiahong, Grosberg, Alexander Yu, & Tanaka, Toyoichi. 1996. Equilibrium swelling properties of polyampholytic hydrogels. *The Journal of chemical physics*, **104**(21), 8713–8720. 1

Geissler, Erik, Hecht, A-M, & Horkay, Ferenc. 2010. Scaling Behavior of Hyaluronic Acid in Solution with Mono-and Divalent Ions. *Pages 362–370 of: Macromolecular symposia*, vol. 291. Wiley Online Library. 1

Ghosh, Snehasish, Li, Xiao, Reed, Christopher E, & Reed, Wayne F. 1990. Apparent persistence lengths and diffusion behavior of high molecular weight hyaluronate. *Biopolymers: Original Research on Biomolecules*, **30**(11-12), 1101–1112. 1

Hill, Terrell L. 1986. *An introduction to statistical thermodynamics*. Courier Corporation. 1, 1, 1

Karamanos, Nikos K, Piperigkou, Zoi, Theocharis, Achilleas D, Watanabe, Hideto, Franchi, Marco, Baud, Stéphanie, Brezillon, Stephane, Gotte, Martin, Passi, Alberto, Vigetti, Davide, *et al.* 2018. Proteoglycan chemical diversity drives multifunctional cell regulation and therapeutics. *Chemical reviews*, **118**(18), 9152–9232. 1

Kaye, Wilbur, & McDaniel, JB. 1974. Low-angle laser light scattering—Rayleigh factors and depolarization ratios. *Applied Optics*, **13**(8), 1934–1937. 3.1

Koushanpour, Esmail. 1976. Renal Physiology: Principles and Functions. *An integrated analysis of renal-body fluid regulating systems*, 242–243. 2.2

Luan, Tu, Fang, Yapeng, Al-Assaf, Saphwan, Phillips, Glyn O, & Zhang, Hongbin. 2011. Compared molecular characterization of hyaluronan using multiple-detection techniques. *Polymer*, **52**(24), 5648–5658. 1, 4.1, 4.2, 8, 5

Morozova, Svetlana, & Muthukumar, Murugappan. 2018. Electrostatic effects in collagen fibril formation. *The Journal of chemical physics*, **149**(16), 163333. 1

Noda, Ichiro, Kato, Narundo, Kitano, Toshiaki, & Nagasawa, Mitsuru. 1981. Thermodynamic properties of moderately concentrated solutions of linear polymers. *Macromolecules*, **14**(3), 668–676. 1, 4.3

Ohta, T, & Oono, Y. 1982. Conformation space renormalization theory of semidilute polymer solutions. *Physics letters A*, **89**(9), 460–464. 1, 4.1, 4.3, 4.3, 5

Schroeder, Daniel V. 1999. *An Introduction to Thermal Physics*. Pearson. Chap. 5. 1

Scott, John E. 1992. The chemical morphology of the vitreous. *Eye*, **6**(6), 553–555. 1

Sebag, J. 1998. Macromolecular structure of the corpus vitreus. *Progress in Polymer Science*, **23**(3), 415–446. 1

Sorci, Gina A, & Reed, Wayne F. 2002. Electrostatically enhanced second and third virial coefficients, viscosity, and interparticle correlations for linear polyelectrolytes. *Macromolecules*, **35**(13), 5218–5227. 3.1

Takahashi, Rheo, Al-Assaf, Saphwan, Williams, Peter A, Kubota, Kenji, Okamoto, Akio, & Nishinari, Katsuyoshi. 2003. Asymmetrical-flow field-flow fractionation with on-line multiangle light scattering detection. 1. Application to wormlike chain analysis of weakly stiff polymer chains. *Biomacromolecules*, **4**(2), 404–409. 4.2

Tavianatou, Anastasia G, Caon, Ilaria, Franchi, Marco, Piperigkou, Zoi, Galesso, Devis, & Karamanos, Nikos K. 2019. Hyaluronan: molecular size-dependent signaling and biological functions in inflammation and cancer. *The FEBS journal*, **286**(15), 2883–2908. 1

Temple-Wong, Michele M, Ren, Shuwen, Quach, Phu, Hansen, Bradley C, Chen, Albert C, Hasegawa, Akihiko, D'Lima, Darryl D, Koziol, Jim, Masuda, Koichi, Lotz, Martin K, *et al.* 2016. Hyaluronan concentration and size distribution in human knee synovial fluid: variations with age and cartilage degeneration. *Arthritis research & therapy*, **18**(1), 1–8. 1

Vrij, A, & Overbeek, J Th G. 1962. Scattering of light by charged colloidal particles in salt solutions. *Journal of colloid science*, **17**(6), 570–588. 3.1

Walls, David. 2019. *Determination of an apparent second virial coefficient for solutions of 1.5 MDa sodium hyaluronate*. Senior project, personal communication. 3.1

Wang, Lixiao, & Bloomfield, Victor A. 1990. Osmotic pressure of semidilute solutions of flexible, globular, and stiff-chain polyelectrolytes with added salt. *Macromolecules*, **23**(1), 194–199. 1, 4.1, 4.3, 4.4

Wiltzius, Pierre, Haller, Hans R, Cannell, David S, & Schaefer, Dale W. 1983. Universality for static properties of polystyrenes in good and marginal solvents. *Physical review letters*, **51**(13), 1183. 1, 4.1, 4.3, 4.3, 4.4

Yamakawa, Hiromi. 1971. *Modern theory of polymer solutions*. Harper & Row. 2.3